MSc in Photonics

PHOTONICS**BCN**

Universitat Politècnica de Catalunya (UPC)
Universitat Autònoma de Barcelona (UAB)
Universitat de Barcelona (UB)
Institut de Ciències Fotòniques (ICFO)

http://www.photonicsbcn.eu

Master in Photonics

MASTER THESIS WORK

QUANTUM FREQUENCY CONVERSION OF SINGLE PHOTONS EMITTED BY ATOMIC QUANTUM MEMORIES TO TELECOM WAVELENGTHS

Pau Farrera Soler

Supervised by Prof. Hugues de Riedmatten, (ICFO)

Presented on date 9th September 2013

Registered at

Escola Tècnica Superior d'Enginyeria de Telecomunicació de Barcelona

Quantum frequency conversion of single photons emitted by atomic quantum memories to telecom wavelengths

Pau Farrera Soler

ICFO - Institut de Ciències Fotòniques, Mediterranean Technology Park, 08860 Castelldefels (Barcelona), Spain

E-mail: Pau.Farrera@icfo.es

Abstract. In quantum repeater schemes for long distance quantum communication, quantum memories (QMs) play a vital role. For these applications, QMs need to be connected to the fiber optics network. However most QMs operate at wavelengths where the absorption in optical fibers is high. Therefore, their connection to a quantum frequency converter (QFC) to telecom wavelengths is required. In this work we convert an heralded single photon emitted by a ^{87}Rb atomic ensemble QM, using a QFC implemented with a non-linear waveguide. The main advantages of this converter setup are its compactness, relative simplicity and wavelength flexibility. We show that after this process the non-classical correlations between the heralding photons and converted heralded photons generated in the QM are preserved. This is the first time that frequency conversion of non-classical light emitted by an atomic QM is performed with a solid state device.

Keywords: quantum repeater, quantum frequency conversion, quantum memory.

1. Introduction

The distribution of entangled states over distant locations is very important in quantum information science. Specifically, it can be used for quantum key distribution protocols and quantum teleportation, amongst others. Nowadays, the most realistic experimental schemes for quantum communication are based on the use of photonic channels, but the transmission distance is limited by the fact that optical absorption increases exponentially with the length of the channels (e.g. optical fibers). The solution used in classical communication to overcome this problem is the use of amplifiers. However, this solution cannot be applied to quantum communication: the no cloning theorem [1] states that a quantum system cannot be copied without degrading its fidelity. To overcome this limitation, several theoretical schemes for quantum repeaters have been proposed [2, 3]. The basic procedure of these protocols is to split the total distance in several sections, distribute entanglement independently in each section, and use entanglement swapping to extend the entanglement over the total distance. In order to perform the entanglement swapping operation, the different sections have to be synchronized (two neighbouring

links need to be entangled at the same time). This leads to two requirements for any quantum repeater scheme: the entanglement needs to be created in a heralded way, and it has to be stored for a programmable time in quantum memories.

For the entanglement creation and swapping operations, QMs need to be connected to optical fibers. However, at present, most of the QMs operate in wavelength ranges that exhibit a significant absorption in optical fibers. For this reason, in order to connect remote QMs efficiently, a device that converts the emitted photons into photons in the telecom band is needed [4, 5]. In Figure 1 we consider the case of a QM based on ^{87}Rb atoms operating with photons at $\lambda = 780\,\text{nm}$ and a QFC that can convert this light to $\lambda = 1550\,\text{nm}$. As it can be observed in Figure 1 (b), even in the case that the conversion process is characterized by an efficiency below 1%, after a few kilometres it allows a higher signal transmission with respect to the non-converted light.

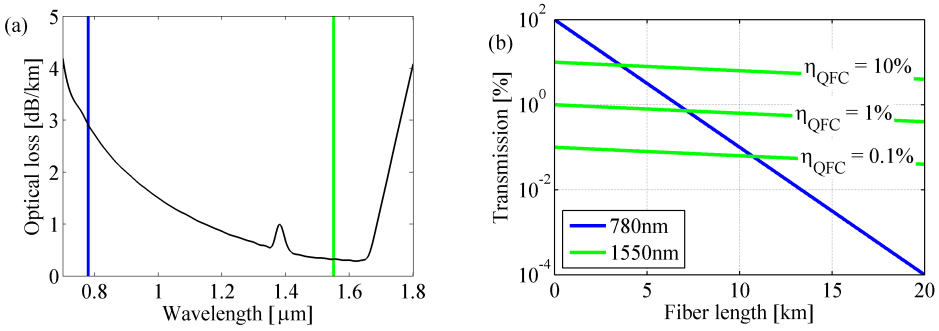

Figure 1. (a) Optical loss in fibers depending on the wavelength of the light. **(b)** Optical fiber transmission efficiency of 780nm light (blue line) and light converted to 1550nm (green lines), representing three different efficiencies of the QFC.

1.1. QMs based on spontaneous Raman scattering

One of the most relevant proposals for quantum repeaters is the Duan-Lukin-Cirac-Zoller (DLCZ) protocol [6], which relies on the creation, storage and transfer to single photons, of single collective spin excitations in atomic ensemble QMs. The atomic level structure relevant for the QM, is a Λ system with two spin ground states ($|g\rangle$ and $|s\rangle$) and an excited state $|e\rangle$. The relevant steps for the entanglement creation and storage are the following.

With all the atoms of the ensemble initially in $|g\rangle$, a write pulse off-resonant on the $|g\rangle - |e\rangle$ transition leads to an emission of a Raman photon (Stokes photon) on the $|e\rangle - |s\rangle$ transition (see Figure 2). This spontaneous Raman scattering process occurs with a certain probability p. The detection of this Stokes photon, projects the state of the ensemble into a superposition of single atomic excitations, called single collective atomic spin excitation

$$\frac{1}{\sqrt{N_A}} \sum_{i=1}^{N_A} e^{i(\vec{k_w} - \vec{k_S})\vec{x_i}} \, |g\rangle_1 \, |g\rangle_2 \cdots |s\rangle_i \cdots |g\rangle_{N_A} \tag{1}$$

where $\vec{k_w}$ and $\vec{k_S}$ are the wave vectors of the write pulse and the Stokes photon respectively, $\vec{x_i}$ is the position of the i-th atom, and N_A is the number of atoms that contribute to the single collective excitation. For the DLCZ protocol the Stokes photon is used to create entanglement between two QMs, and the atomic excitation allows to store it. After a programmable time τ (storage time), a pulse resonant on the $|s\rangle - |e\rangle$ transition (read pulse) is applied. The system can decay to the initial state $|g\rangle$, emitting a photon on the $|e\rangle - |g\rangle$ transition (anti-Stokes photon). Taking into account the phases acquired in the process, the final state of the atomic ensemble can be written as follows

$$\frac{1}{\sqrt{N_A}} \sum_{i=1}^{N_A} e^{i(\vec{k_w} - \vec{k_S})\vec{x_i}} e^{i(\vec{k_r} - \vec{k_{AS}})\vec{x_i'}} |g\rangle_1 |g\rangle_2 \cdots |g\rangle_i \cdots |g\rangle_{N_A} \tag{2}$$

where $\vec{x_i'}$ is the position of the i-th atom at the moment of the read-out process. If the atoms are not moving during the storage time ($\vec{x_i} = \vec{x_i'}$), the phase matching condition that leads to constructive interference is $\vec{k_{AS}} = \vec{k_w} + \vec{k_r} - \vec{k_S}$. This collective interference effect allows us to convert the spin excitation into an anti-Stokes photon in a well-defined direction and with high efficiency. Cold atomic ensembles are therefore good candidates for QMs. This efficient conversion of the atomic excitation to an anti-Stokes photon is used for the entanglement swapping operation.

Depending on the power of the pulses and the density of the atomic ensemble, several atoms can be excited and different numbers of S-AS photon pairs can be created. Due to the high correlation between Stokes photons and collective spin excitations, and considering a highly efficient read-out process, the state for the Stokes and anti-Stokes modes is ideally a two mode squeezed state $\sqrt{1-p}(|0_S, 0_{AS}\rangle + \sqrt{p}\,|1_S, 1_{AS}\rangle + p\,|2_S, 2_{AS}\rangle + 0(p^{3/2}))$. For this state, the normalized second order cross-correlation function of the Stokes and anti-Stokes modes is related with p as $g^{(2)}_{S,AS} = 1 + \frac{1}{p}$ [7]. It has been shown [7] that there exists a bound for classical fields which can be obtained from the Cauchy-Schwarz inequality:

$$g^{(2)}_{S,AS} \leq \sqrt{g^{(2)}_{S,S}\, g^{(2)}_{AS,AS}} \tag{3}$$

where $g^{(2)}_{S,S}$ and $g^{(2)}_{AS,AS}$ are the normalized second order autocorrelation functions of the Stokes and the anti-Stokes fields, respectively. For a perfect two mode squeezed state, both Stokes and anti-Stokes fields should exhibit thermal statistics, with $g^{(2)}_{S,S} = g^{(2)}_{AS,AS} = 2$. In this case measuring $g^{(2)}_{S,AS} > 2$ is a strong indication of non-classical correlation between the two modes.

1.2. The quantum frequency converter (QFC)

As explained in section 1.1, in order to efficiently connect remote quantum memories, it is important to translate the frequency of the emitted photons to a spectral region suitable for optical fiber networks. In this context, there are three requirements regarding the conversion process that any QFC setup should fulfil: (1) to preserve the quantum properties of the photons, (2) to perform the frequency conversion with a high efficiency,

and (3) to add the lowest level of noise possible (a single photon level of the noise is necessary). An experiment showing the quantum frequency conversion of light from a QM has been reported recently using four wave mixing in a dense cold atomic ensemble [8]. However this technique requires a complex experimental setup, and is restricted to wavelengths close to atomic transitions. In our experiment we use a QFC setup based on difference frequency generation (DFG), in a periodically poled lithium niobate (PPLN) waveguide [9]. In particular, we want to convert the anti-Stokes photons emitted by our ^{87}Rb QM (at $\lambda_{AS} = 780.2\,\text{nm}$) using pump light at $\lambda_p = 1569\,\text{nm}$. The wavelength of the converted anti-Stokes is determined by the energy conservation of the process $\left(\frac{1}{\lambda_{cAS}} = \frac{1}{\lambda_{AS}} - \frac{1}{\lambda_p}\right)$, which gives $\lambda_{cAS} = 1552\,\text{nm}$. The two relevant parameters to characterize the system are the efficiency of the conversion (η_{QFC}), and the signal to noise ratio (SNR) of the converted signal. A good figure of merit combining these two parameters is the mean input photon number μ_1 to obtain SNR = 1. This QFC setup is the result of two previous Master theses in the group [10, 11]. The state of the art at the moment of my arrival was $\mu_1 = 0.7 \pm 0.1$ [9].

1.3. Objectives

The aim of this project is to convert non-classical light coming from a ^{87}Rb atomic ensemble QM, to a wavelength in the telecom range. In particular, we want to show that quantum correlations between the Stokes and anti-Stokes photons survive the frequency conversion. For this purpose the QFC setup and the QM had to be optimized in order to preserve the quantum nature of the photons during the conversion process.

2. Experimental procedure and results

2.1. Experimental setup

The essential elements of the experimental setup are shown in Figure 2. An ensemble of cold ^{87}Rb atoms is created using a magneto-optical trap (MOT). The atomic three-level Λ system used for the write-read process involves the two ground states $|g\rangle = \left|5^2S_{1/2}, F = 1\right\rangle$ and $|s\rangle = \left|5^2S_{1/2}, F = 2\right\rangle$, and the excited state $|e\rangle = \left|5^2S_{3/2}, F = 2\right\rangle$. In order to filter the Stokes photons from the write light (detuned by 6.8 GHz), the Stokes mode is coupled into a single mode fiber (SMF) oriented with an angle of 3° with respect to the write beam. Furthermore, two additional filtering methods are used: a polarization filtering system consisting on two polarizing beam splitters (PBSs) and a $\lambda/2$ waveplate (HWP), and a monolithic cavity with $\sim 100\,\text{MHz}$ linewidth for spectral filtering. Following these filtering stages, the Stokes photon is sent to the single photon detector (SPD) D_S, which is a Si avalanche photodiode (detection efficiency $\eta_{D,Si} = 0.43$ and dark counts rate DCR = 70Hz). Since the write and read pulses are chosen to be counterpropagating, the phase matching condition (section 1.1) sets the direction of the anti-Stokes photon opposed to the direction of the correlated Stokes mode. When the QM is not used in combination with the QFC, the anti-Stokes photon is coupled into

a SMF and sent to the SPD D_{AS} (similar to D_S). The outputs of both SPDs are sent to a time stamping module which can record their arrival times with subnanosecond resolution.

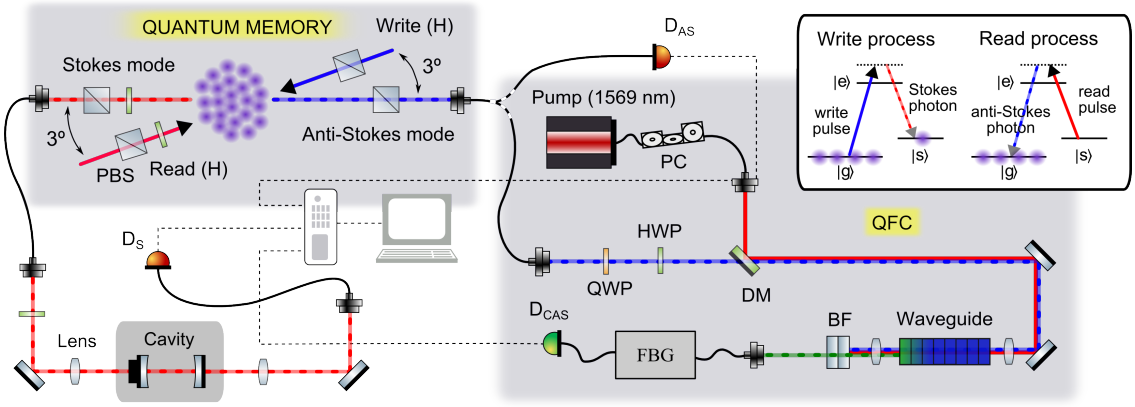

Figure 2. Experimental setup used to measure DLCZ correlations, including the QFC setup used to convert the anti-Stokes photons.

For the conversion of the heralded anti-Stokes photons we use the mentioned waveguide-based QFC setup. The 780.2 nm photon goes through a $\lambda/4$ waveplate (QWP) and a $\lambda/2$ waveplate to adjust its polarization, and is overlapped with the pump beam (1569 nm) on a dichroic mirror (DM). The pump light is generated by an external cavity diode laser, and before reaching the DM, it passes through a polarization controller (PC). Both fields are then coupled to the PPLN waveguide where the DFG process takes place. The converted photons at $\lambda_{cAS} = 1552\,\text{nm}$ are sent afterwards to two filtering stages in order to reduce the noise originated by the pump beam. Firstly, the light passes through two band-pass filters (BF) with $\Delta\lambda = 3\,\text{nm}$ that filter out the residual pump light. Secondly, after coupling to a SMF, a Fiber Bragg grating with $\Delta\nu = 2.5\,\text{GHz}$ and a maximum transmission of 77 % filters out most of the broadband noise due to Raman scattering of the pump. Finally, the output light is sent to a InGaAs SPD with $\eta_{D,InGaAs} = 0.1$ and DCR $= 540\,\text{Hz}$, which is also connected to the time stamping module.

2.2. Experimental sequence

In order to quantify the degree of correlation between the Stokes and the anti-Stokes photons, we use the cross-correlation function $g^{(2)}_{S,AS}$ introduced in section 1.1. The main features of the experimental sequence are explained in the following lines (see Figure 3). As already mentioned, in order to have an efficient read-out process we need to cool and trap the atoms in a MOT. However, the MOT cannot be operated during the measurement for the reason that it would shuffle the populations of the atomic levels, and destroy the single spin excitations. To avoid this, the MOT is switched off for a time ΔT. During this period, N write-read trials are performed. Optical pumping (OP) at

the beginning of each trial prepares all the atoms of the ensemble in the ground level $|g\rangle$. In order to limit the effect of noise, both SPDs for the Stokes and anti-Stokes photons are gated only for a short time given by the length of the write and read pulses (of the order of tens of nanoseconds). When the N-th trial is finished the atoms are retrapped in the MOT, and the procedure is iterated until good statistics are reached.

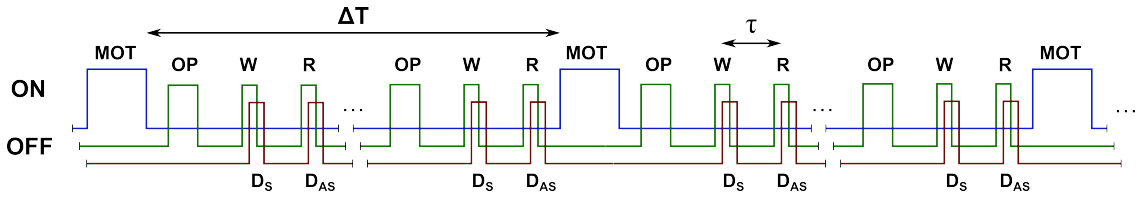

Figure 3. Scheme with the main features of the sequence used to measure $g^{(2)}_{S,AS}$.

2.3. DLCZ correlations

In order calculate the S-AS cross-correlation function, we use the expression $g^{(2)}_{S,AS} = \frac{p_{S,AS}}{p_S p_{AS}}$, where $p_{S(AS)}$ is the Stokes (anti-Stokes) detection probability and $p_{S,AS}$ is the probability to detect both photons in the same write-read trial. Another important parameter to characterize the setup is the retrieval efficiency η_R of the stored excitation, defined as the probability to have an anti-Stokes photon in a SMF conditioned on a Stokes detection. Figure 4 shows the experimental data for $g^{(2)}_{S,AS}$ and η_R as a function of the Stokes detection probability, which is varied changing the write pulse energy.

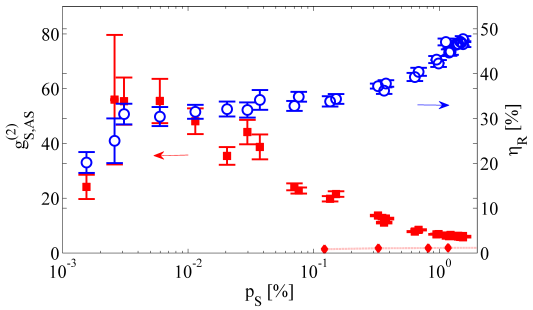

Figure 4. S-AS cross-correlation function (red squares) as a function of the Stokes photon detection probability, with its classical bound (red diamonds). The blue circles represent the retrieval efficiency. The storage time is $\tau = 330$ ns.

This measurement is only corrected for the detection efficiency of the SPDs ($\eta_{D,Si} = 0.43$). The anti-Stokes photons optical transmission before reaching the SPD is characterized by a transmission efficiency $\eta_t^{AS} = 0.60$. This gives an intrinsic retrieval efficiency around 53% (corresponding to a measured $\eta_R = 32\%$). As it can be appreciated, the cross-correlation function increases as the Stokes detection probability decreases (as described in section 1.1). For low values of p_S the dark counts of the detector become significant and $g^{(2)}_{S,AS}$ decreases. The retrieval efficiency

remains constant in the single excitation regime, and increases for high values of p_S as a consequence of multiexcitation processes. The red diamonds represent the classical bound for the $g^{(2)}_{S,AS}$, given by eq. 3. As it can be seen, our measurements exhibit a clear violation of the Cauchy-Schwarz inequality (eq. 3) and are a proof of non-classical correlations.

Another interesting characteristics of this experiment is that the detection of a Stokes photon projects the anti-Stokes field on a single photon state. This state can be characterized with a Hanbury-Brown-Twiss setup, placing a 50/50 beam splitter in the path of the anti-Stokes field and sending the two output modes to two SPDs $D_{AS,1}$ and $D_{AS,2}$. The quality of this heralded single photon state can be assessed with the anticorrelation parameter α

$$\alpha = \frac{p_{(1,2|S)}}{p_{(1|S)}p_{(2|S)}} \tag{4}$$

where with the notation $p_{(...|S)}$ we indicate that the probabilities are conditioned on a Stokes photon detection. Measuring the anticorrelation parameter using a similar sequence as for $g^{(2)}_{S,AS}$, gives us a value $\alpha = 0.2 \pm 0.2$ corresponding to $p_S = 0.07\%$. Since classical fields should follow the inequality $\alpha \geq 1$ [12], this is a proof of non-classical light and a distinct sign of the antibunching effect, characteristic of single photon states.

2.4. QFC characterization

A complete characterization of the QFC setup can be found in [9, 10]. In this section we show the measurements relevant for its connection with the quantum memory. As already mentioned, the two relevant parameters to characterize the system are η_{QFC} and the SNR of the converted signal. In order to measure these quantities we send to the

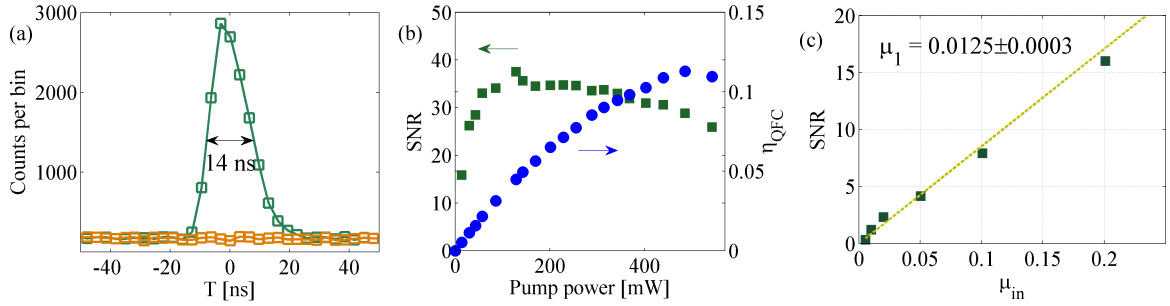

Figure 5. **(a)** Typical measurement of the converted signal (in green) and noise (in orange). **(b)** Efficiency of the QFC and SNR for different values of the pump power (measured before the waveguide). **(c)** Measured SNR after the whole conversion process (including filtering stages) for different average input number of photons per pulse. For figures (b) and (c) the detection gate width is 20 ns.

QFC setup coherent laser pulses attenuated to the single photon level, mimicking the anti-Stokes photons. After passing through the filtering stages, we measure two different quantities with the SPD: the noise (which is measured in absence of input signal and

includes pump noise and detector dark counts), and the total converted signal (which includes the converted photons and the noise). To calculate η_{QFC}, we divide the number of detected converted photons (with noise subtracted) by the number of signal photons at the input of the waveguide (μ_{in}), and compensate for $\eta_{D,InGaAs} = 0.1$. For the SNR, we divide the converted signal (also with noise subtracted), by the noise.

Figure 5 (b) shows η_{QFC} and the SNR as a function of the pump beam power, for input pulses of FWHM = 14 ns and an average input number of photons $\mu_{in} = 0.37$. Around 350 mW we have a good trade off between η_{QFC} and the SNR. Unless otherwise specified, in the following measurements we use this pump power. This is the case of the data shown in Figure 5 (c), where the SNR is measured for pulses with different μ_{in}. This measurement allows to calculate the value $\mu_1 = 0.0125 \pm 0.0003$.

2.5. DLCZ correlations converting the anti-Stokes photons

After characterizing the QM and the QFC we show the results obtained by combining both setups. In Figure 6 we can see the converted anti-Stokes counts that follow a Stokes detection, in a $g^{(2)QFC}_{S,AS}$ measurement with $p_S = 0.15\%$. A trigger signal at a fixed time, conditioned on a Stokes detection allows us to record the correlated anti-Stokes photon shape. The red circles correspond to a measurement where the anti-Stokes photons are blocked before reaching the QFC. In other words, they represent the coincidences between a Stokes detection and the detection of a photon coming from the pump noise.

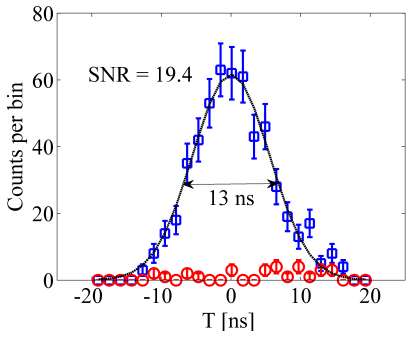

Figure 6. S-AS coincidences following the anti-Stokes photon shape (blue squares). The red circles, correspond to the coincidences where the stop count is due to a pump noise photon instead of an anti-Stokes photon.

In a DLCZ quantum repeater experiment, the counts in red would be the noise that the pump laser would introduce to the entanglement swapping operation, and one limitation for the fidelity of the protocol. Nevertheless, the SNR we obtain is reasonably high. From this measurement we can calculate an upper bound for the cross-correlation function, dividing the S-AS coincidences by the S-noise ones, which gives $g^{(2)QFC}_{S,AS} \leq 19.4$. This would be the limitation that the pump noise introduces to the $g^{(2)QFC}_{S,AS}$ value.

Taking into account that the anti-Stokes photons conversion process adds noise to their detection (quantified by the μ_1), it can be shown that the expected value for the

S-AS cross-correlation function after conversion is

$$g^{(2)QFC}_{S,AS} = g^{(2)}_{S,AS}\frac{\eta^{in}_R + \mu_1}{\eta^{in}_R + g^{(2)}_{S,AS}\mu_1} \tag{5}$$

where η^{in}_R stands for the retrieval efficiency, compensated for the losses until the input of the waveguide. For sufficiently high values of $g^{(2)}_{S,AS}$, the upper bound for the cross-correlation function after conversion is $g^{(2)QFC}_{S,AS} = 1 + \frac{\eta^{in}_R}{\mu_1}$. Compensating for the losses the retrieval efficiency that we show in Figure 4 (around 32%), we obtain that in our experiment we have $\eta^{in}_R = 24.7\%$. Hence, for the value $\mu_1 = 0.0125$ (see section 2.4), we get that the maximum achievable $g^{(2)}_{S,AS}$ value after conversion is $g^{(2)QFC}_{S,AS} \approx 20$. This value is in accordance with the one obtained previously using the data in Figure 6. The measurements of the $g^{(2)QFC}_{S,AS}$ as a function of p_S are shown in Figure 7 (a).

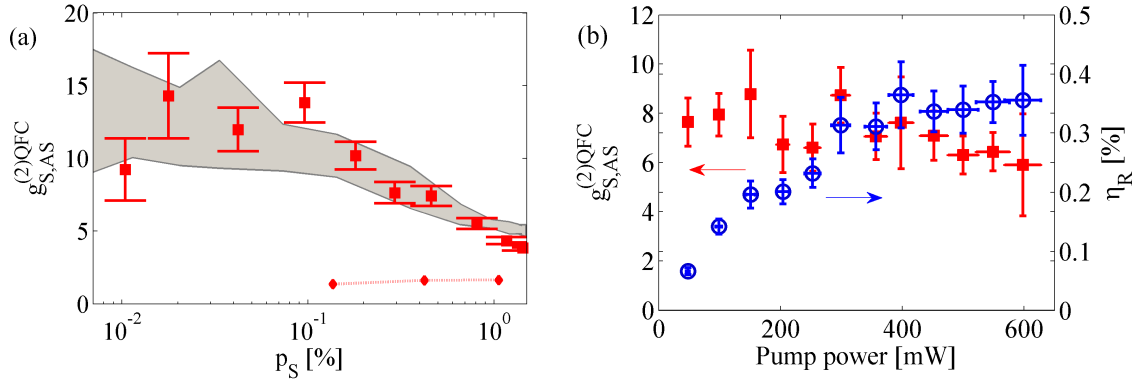

Figure 7. (a) $g^{(2)QFC}_{S,AS}$ measured after the anti-Stokes conversion, when varying the write pulse energy and **(b)** the pump power. The blue circles represent the measured retrieval efficiency after the anti-Stokes photons conversion and detection.

The grey shadow represents the expected values for $g^{(2)QFC}_{S,AS}$. They are calculated with eq. 5, using the values of $g^{(2)}_{S,AS}$, η_R and μ_1 shown in Figures 4 and 5 (c). In a similar way as in Figure 4, the red diamonds represent the classical bound for the $g^{(2)QFC}_{S,AS}$. Since our measurements violate widely the Cauchy-Schwarz inequality (eq. 3), we can claim that the non-classical correlation between the two fields is clearly preserved after the anti-Stokes frequency conversion. In Figure 7 (b) we show the $g^{(2)QFC}_{S,AS}$ for different pump powers and a fixed $p_S = 0.3\%$. The conditional efficiency to detect a converted anti-Stokes photon given a Stokes detection is also shown (blue circles). It can be appreciated that η_R follows the behaviour of η_{QFC} shown in Figure 5 (b), while the $g^{(2)QFC}_{S,AS}$ follows the SNR. This is the behaviour expected taking into account eq. 5.

3. Conclusion and further work

We have reported the conversion of non-classical light coming from a ^{87}Rb atomic ensemble quantum memory at 780.2 nm to the telecom wavelength 1552 nm. This is

an important achievement in the context of the experimental realization of quantum repeater protocols. In the characterization of the QM we have obtained a high amount of non-classical correlations between the Stokes and the anti-Stokes fields (up to $g^{(2)}_{S,AS} = 56 \pm 8$) and an intrinsic retrieval efficiency of 53%. Concerning the QFC setup we have measured a device conversion efficiency of $\eta_{QFC} = 10\%$ and a SNR quantified by $\mu_1 = 0.0125 \pm 0.0003$. These parameters have enabled us to observe non-classical correlations after the conversion of the anti-Stokes photons (up to $g^{(2)QFC}_{S,AS} = 14 \pm 3$). Knowing that the μ_1 is directly related with the cross-correlation function after conversion (eq. 5), and that most of the noise in the QFC is broadband [9], we have plans to install an etalon of $\Delta\nu = 100\,\mathrm{MHz}$ after the waveguide, to reduce μ_1. We are also planning to mount an optical cavity around our QM, that would enhance the conversion of the atomic excitations to anti-Stokes photons, and increase η_R [13].

4. Acknowledgements

I would like to express my deep gratitude to Prof. Hugues de Riedmatten for giving me the opportunity of joining the Quantum Photonics with Solids and Atoms group and for his guidance during my master thesis. I am particularly grateful as well to Matteo Cristiani for his teachings and support, and to Boris Albrecht with whom I have worked very close and from whom I have learnt a lot. Thanks also to the rest of the QPSA group who helped me in this experience and to CX CatalunyaCaixa Fundació for financial support.

References

[1] Wootters, W. K., and Zurek, W. H.; Nature, 1982, 299, 802
[2] Briegel, H.-J.; Dür, W.; Cirac, J. I., and Zoller, P.; Phys. Rev. Lett., 1998, 81, 5932-5935
[3] Sangouard, N.; Simon, C.; de Riedmatten, H., and Gisin, N.; Rev. Mod. Phys., 2011, 83, 33-80
[4] Curtz, N.; Thew, R.; Simon, C.; Gisin, N., and Zbinden, H.; Opt. Express, 2010, 18, 22099-22104
[5] Takesue, H.; Phys. Rev. A, 2010, 82, 013833
[6] Duan, L.-M.; Lukin, M. D.; Cirac, J. I., and Zoller, P.; Nature, 2001, 414, 413-418
[7] Kuzmich, A.; Bowen, W. P.; Boozer, A. D.; Boca, A.; Chou, C. W.; Duan, L.-M., and Kimble, H. J.; Nature, 2003, 423, 731-734
[8] Radnaev, A. G.; Dudin, Y. O.; Zhao, R.; Jen, H. H.; Jenkins, S. D.; Kuzmich, A., and Kennedy, T. A. B.; Nature Physics, 2010, 6, 894-899
[9] Fernandez-Gonzalvo, X.; Corrielli, G.; Albrecht, B.; Grimau, M.; Cristiani, M. and de Riedmatten, H. Opt. Express, 2013, 21, 19473-19487
[10] Fernandez, X.; "Characterization of a quantum frequency converter for quantum repeater applications" Universitat Politcnica de Catalunya, 2012
[11] Corrielli, G.; " Towards frequency conversion of quantum memory compatible photons for quantum repeater applications" Politecnico di Milano, 2011
[12] Loudon, R.; "The Quantum Theory of Light" (Oxford Science Publications) Oxford University Press, USA, 2000
[13] Bao, X.-H.; Reingruber, A.; Dietrich, P.; Rui, J.; Dück, A.; Strassel, T.; Li, L.; Liu, N.-L.; Zhao, B., and Pan, J.-W.; Nature Physics, 2012, 8, 517-521